Materials Today Bio 31 (2025) 101588

Contents lists available at ScienceDirect

Materials Today Bio

journal homepage: www.journals.elsevier.com/materials-today-bio

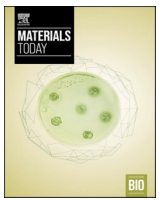

Multifunctional hydrogel loaded with 4-octyl itaconate and exosomes to induce bone regeneration for diabetic infected bone defect via Keap1-Nrf2 pathway☆

Yizhou Wan *, Qing Gao, Bing Ye, Wenzhe Sun, Kaifang Chen **, Xiaodong Guo ***

Department of Orthopaedics, Union Hospital, Tongji Medical College, Huazhong University of Science & Technology, 1277 Jiefang Avenue, Wuhan, 430022, China

ARTICLE INFO

Keywords:
4-Octyl itaconate
Exosomes
Diabetic infected bone defect
Innervation
Vascularization

ABSTRACT

Diabetic infected bone defect remains a great challenge in clinical practice, with delayed healing characterized by bacterial infection and cellular disfunction caused by oxidative stress. Hence, a novel self-healing multifunctional Ag@PEG-4OI/EXO hydrogel is introduced for improving healing of diabetic infected bone defect. 4-octyl itaconate, a derivative of the metabolite itaconate, has been proved that which performs antioxidant and mitochondria-protected properties. Simultaneously, the Ag^{+} that performed as cross-linking agent binds 4-arm-PEG-SH to form anti-bacterial hydrogel to deliver the bioactive molecule. The released of 4OI is confirmed that it can alleviate excessive ROS damage to cells and protect mitochondrial functions according to Keap1-Nrf2 pathway, synergistically promoting neurovascularization and osteogenic differentiation with EXO (from repair Schwann cells). In vivo, the Ag@PEG-4OI/EXO hydrogel also shows ideal antibacterial property and ameliorate the microenvironment of cells, finally promoting regeneration of $CGRP^{+}$ nerve fibers and bone healing. In vivo and in vitro studies demonstrate that the improvement functions of cells with the use of the Ag@PEG-4OI/EXO hydrogel, presenting a viable strategy for diabetic infected bone defect.

1. Introduction

Diabetes mellitus (DM) is one of the chronic metabolic diseases that affected 387 million people in 2013 [1]. Moreover, as the increasing of obese and elder population, more than 590 million global individuals would be affected by DM by the year 2035 [2]. In addition, some clinical studies reveal that patients with DM have higher risk of infection than normal people in the process of bone regeneration, which eventually causes the failure of surgery [3]. The balance of oxidation-antioxidant system is destroyed in the bone microenvironment with DM and infection by toxins secreted by bacteria and excessive reactive oxygen species (ROS) induced by DM [4,5]. These above factors inhibit cell proliferation and differentiation and improve necrosis of blood vessels and verve fibers [6], finally impeding bone repair. Hence, to put forward novel treatment strategies to improve bone regeneration ability in diabetic microenvironment is urgently demanded.

The crosstalk between abundant nerves and vessels in natural bone regeneration microenvironment constitutes the nerve-vessel network, which plays an important role in inducing osteogenic differentiation of endogenous bone marrow mesenchymal cells [7–9]. Besides, growing studies reveal that in process of bone repair, the nerve regeneration peaks firstly after fracture-before vascularization, ossification and mineralization and subsequently initiates bone repair [8,10]. Regenerated nerves secret neuropeptides such as calcitonin gene-related peptide (CGRP) to promote vascularization [11,12], and the regenerated blood vessels will secret nerve growth factor (NGF) to promote neuralization [13], finally regulating bone repair. However, in diabetic infected microenvironment, the excessive ROS, inflammatory factors and bacterial productions will impede bone repair according to different ways such as weakened differentiation, decreased angiogenesis and

Abbreviations: 4OI, 4-octyl itaconate; BV/TV, Bone-to-tissue volume ratio; BMSCs, Bone marrow mesenchymal stem cells; DM, Diabetes mellitus; EXOs, Exosomes; HUVECs, Human vascular endothelial cells; PNS, Peripheral nervous system; ROS, Reactive oxygen species; SCs, Schwann cell.

☆ Funded by the National Natural Science Foundation of China (grants No. 82272446).

* Corresponding author.
** Corresponding author.
*** Corresponding author.
E-mail addresses: 651058382@163.com (Y. Wan), ckf@hust.edu.cn (K. Chen), xiaodongguo@hust.edu.cn (X. Guo).

https://doi.org/10.1016/j.mtbio.2025.101588
Received 2 December 2024; Received in revised form 9 February 2025; Accepted 16 February 2025
Available online 19 February 2025

neuralization [14–16]. Notably, once the infection is compromised, the remaining ROS produced by DM is the key question should be solved, because it will facilitate the activation migration of inflammatory cells to the area of bone defect and finally delay bone repair [17].

Recent studies reveal that some metabolic intermediates such as itaconate, citric acid and α-ketoglutaric acid are dispensable parts in the process of tissue repairing according to regulate mitochondrial membrane potential [18,19]. 4-octyl itaconate (4OI), a derivative from itaconate in the process of endogenous metabolite, has recently attracted wide attention owing to its well-known functions of immunerегulation and cell-protection [20,21]. As reported by Mills et al., in 2018 [22], after the macrophages induced by lipopolysaccharide (LPS), 4OI can regulate the generation of inflammatory factor (interleukin (IL)-1β) according to kelch-like ECH-associated protein 1 (Keap1)-nuclear erythroid 2-related factor 2 (Nrf2) signal pathway by alkylating Keap1. Liu et al. [23] find that 4OI can reduce the cell death, ROS, and lipid oxidation that induced by H_2O_2. Besedes, another studies report that itaconate can activate the Keap1-Nrf2 pathway [24], inhibit the activation of succinate dehydrogenase (SDH) [25], significantly reduce the level of ROS and malonaldehyde to protect tissue from ischemia reperfusion injury. Hence, 4OI might have similar function for involved cells in the process of bone defect repair in diabetic microenvironment.

Despite the 4OI can protect the cell from oxidative stress injury, yet the function is still less than normal bone regeneration microenvironment [26]. Exosomes (EXOs), a type of extracellular vesicles secreted by cells and contain complex RNAs and proteins, has similar function of secretor and also participates in intercellular communication and the microenvironment [27,28]. Recent studies show that EXO from Schwann cells (SCs) can regulate periphery nerves regeneration [29,30]. Peripheral nerves consist of bundles of axons, with each axon associated and enveloped by SCs [31]. Once the periphery nerves are damaged, the SCs in both the proximal stump and throughout the nerve downstream of the cut will be switched to repair SCs under the stimulation of the transcription factor C-JUN [9,32,33], which clears the debris, remodels

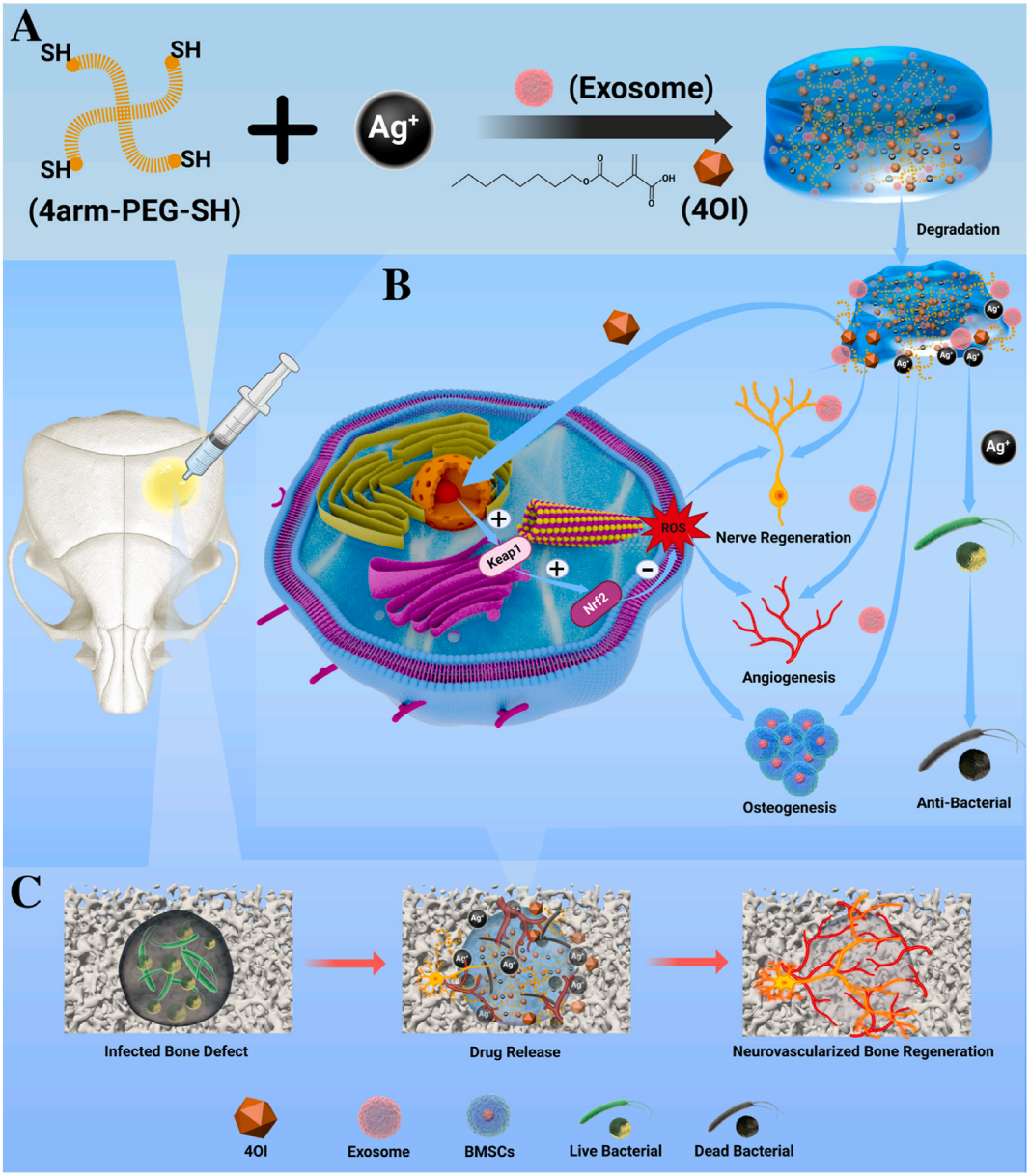

Fig. 1. Schematic illustrations of the synthesis of Ag@PEG-4OI/EXO hydrogel and applied for antibacterial and neurovascularized bone regeneration of infected diabetic bone defect. **(A)** The formation process of Ag@PEG-4OI/EXO hydrogel. **(B)** The mechanism of hydrogel to promote tissue regeneration. **(C)** The repair process of diabetic infected bone defect.

the environment and promote the axonal regeneration. Besides, compared with SCs, the repair SCs possess more effective in regulating nerves regeneration [34]. Therefore, the EXO from repair SCs might be more powerful for the repair of periphery nerves and other tissues regeneration.

In this study, we introduced an injectable hydrogel consisted by dynamic Ag-S coordination bonds between the AgCl and 4-arm-PEG-SH [35], and simultaneously loading with EXO and 4OI, so that this hydrogel will exhibit anti-bacterial, anti-oxidant, mitochondrial protection and tissue regeneration properties (Fig. 1). We expect that this multifunctional "all-in" hydrogel will effectively reverse oxidative stress and eventually promote repair of periphery nerves, vessels and bone defect.

2. Methods

2.1. Induction of and repair SCs EXO extraction

Firstly, the repair SCs should be established. Medium containing 2 ng/mL TGF-β was used to stimulate the formation of repair SCs from SCs, the sustaining time was 3h [9,36]. Once the induction was completed and successful, the repair SCs were cultured for 1 day, and then the supernatant was used for EXO extraction.

The supernatant was moved to centrifuge tube, 10000g at 4 °C for 30 min to remove cell debris and precipitates. The centrifuged supernatant was removed to 0.22 μm filter membrane filtration and filtrate was collected. The filtrate was transferred to a new centrifuge tube and centrifuged at 4 °C, 120000g, for 90 min. Then, the supernatant was removed and the EXO were re-suspended with PBS and stored at −80 °C for subsequent identification and study.

2.2. Synthesis of hydrogels

The 4-arm-PEG-SH (ZhenzhunBiotech Co., Ltd., China) powder was selected as the basic material for the hydrogel synthesis. The 4-arm-PEG-SH solution was prepared by dissolving 50 mg 4-arm-PEG-SH powder in 250 μL deionized water (DI water). Concurrently, 25 μL $AgNO_3$ (0.1 M) was added to 225 μL DI water to prepare $AgNO_3$ solution. The two above solutions were mixed and vibrated to form transparent hydrogel named with Ag@PEG. Then, the 4OI (HY-112675; MCE, China) was dissolved in DMSO with concentration of 10 mM. The 4OI and extracted EXO were separately diluted in DI water with concentration of 50 μM and $3*10^5$/mL to substituted DI water in 4-arm-PEG-SH solution, respectively. Finally, these Ag@PEG hydrogels that loaded with 4OI or EXO were named with Ag@PEG-4OI, Ag@PEG-EXO and Ag@PEG-4OI/EXOs, respectively.

2.3. Self-healing properties of hydrogels

To visualize the self-healing property of hydrogel, the smart phone was used to take photos. The 500 μL hydrogel was placed on the table and divided with ruler into two parts at an interval of 2 mm. The divided two parts would fuse and form individual after 30 s.

2.4. Hygroscopicity of hydrogels

To evaluate the water absorption capability of these hydrogels, the different hydrogels were freeze-dried in vacuum and weighed (W0). Then, these freeze-dried hydrogels were soaked in PBS solution at 37 °C and weighted at 0 min, 30 min, 1 h, 2 h, 4 h, and 12 h to obtain the swollen weight (Wt). The hygroscopicity of hydrogels was calculated using equation [(Wt-W0/W0) * 100 %].

2.5. Rheological test

To evaluate the rheological property of hydrogels, rheometer (Kinexus, Malvern) was used to measure. Frequency scanning of 0.1–10 Hz was performed for different hydrogels, the storage modulus (G′) and loss modulus (G″) were obtained to calculate the rheological property of the hydrogels.

2.6. Morphological characterization of hydrogels

To visualize the morphology of different hydrogels, the scanning electron microscope (SEM) (JSM7600F; JEOL Ltd., Japan) was used. Before the SEM test, these hydrogels should be freeze-dried in vacuum and coated with gold powders.

2.7. Degradation behavior in vitro

To detect the degradation speed of these hydrogels, the hydrogels were firstly immersed in PBS at 37 °C until the hygroscopicity reached equilibrium and the weight was obtained subsequently (W0). The swollen hydrogels were continuously immersed in PBS and weighed every 2 days for 14 days (Wt). The degradation rate of hydrogels was calculated at last by using the equation [(W0 - Wt)/W0*100 %].

2.8. Drug release behavior in vitro

To detect the kinetics of 4OI and Ag^+ release, 500 μL hydrogels were immersed in 2 mL PBS at 37 °C with gentle vibrating. The solutions were collected at 3, 12 24 h and 2, 4, 7 d. The released Ag^+ was detected by mass spectrometer (NexION 2000, PerkinElmer, USA), and the 4OI was detected by ultraviolet spectrophotometer (UV- 2700, Shimadzu, Japan).

2.9. Preparation of hydrogels extract

Different hydrogels were immersed in fresh Dulbecco's modified Eagle's medium (Gibco, Grand Island, NY, USA) in 50-mL centrifuge tube and incubated for 48 h at 37 °C according to the previous studies [37]. Then, the extracts were processed with 0.22-μm filters for disinfection, and 10 % FBS, 1 % penicillin and streptomycin (Gibco, USA) were added to the medium before application. The prepared hydrogels extract of Ag@PEG, Ag@PEG-4OI, Ag@PEG-EXO and Ag@PEG-4OI + EXO were named as Ag, 4OI, EXO and 4OI + EXOs.

2.10. In vitro antibacterial assays

The *Staphylococcus aureus* (gram-positive bacterium) and *Escherichia coli* (gram-negative bacterium) were used to detect the antibacterial effect of hydrogels in vitro. The 10 mL extract of different hydrogels (Ag@PEG, Ag@PEG-4OI, Ag@PEG-EXO and Ag@PEG-4OI/EXOs) were used to suspend the bacterial with concentration of $1*10^6$ CFU/mL and incubated for 3 h at 37 °C. The bacteria suspended with PBS was set as control. Then, 100 μL incubated suspensions of bacteria were cultured on solid agar plates and the number of colonies were counted after incubation for 12 h. The antibacterial effect was evaluated by equation [N/C*100 %], the N represented the hydrogels groups, the C represented the control group. To evaluate the viability of bacteria in different suspensions, the SYTO 9/PI staining was performed and the results were observed under fluorescence microscopy (Olympus IX73). In addition, to further observe the morphology of bacteria in different suspension, the SME was performed. Before the SEM performed, the bacteria must be fixed with 4 % glutaraldehyde for 4 h at 4 °C, dehydrated with ethanol solution and freeze-dried.

2.11. Cytocompatibility assays

To detect the toxicity of different hydrogels, the cell live/dead staining assays were performed. Cells were cultured in 24-well plate at a density of 1×10^4/mL with different hydrogel extracts. After 1 and 2

days of culturing, the live-dead assay was performed according to the manufacturer's instruction. The stained samples were observed under fluorescence microscope. In addition, cell proliferation was evaluated by the CCK8 assay (Beyotime, China) at day 1, 2, 3 after seeding according to the manufacturer's instruction.

2.12. Evaluation of intracellular ROS scavenging function

To detect the intracellular ROS level, the DCFH-DA was used as staining probe. $1*10^5$ cells/well were seeded in 6-well plates and cultured with the hydrogels extract medium for 24 h. Then, the tert-butyl hydroperoxide (tBHP; 458,139; Sigma, USA) was used to treat cells for 3 h to induce oxidative stress statue. Cells in the 6-well plates that treated without extracts or tBHP was set as control group. Next, the 10 μM DCFH-DA (Beyotime, China) was added and incubated in cell incubator for 20 min. After rinsed with PBS for 3 times, the cells were observed under fluorescence microscope. In addition, the Annexin V-FITC Apoptosis Detection Kit (Elabscience, Biotechnology Co., Ltd, China) was used to detect the cell apoptosis. Then, cells were collected to quantitatively detect the ROS and apoptosis by flow cytometer.

2.13. Mitochondrial membrane potential detection

$1*10^5$ Cells were seeded in confocal dish and cultured with extracts medium for 24 h. After that, the t-BPH was used to treat cell for 3 h. The MitoTracter Red (#C1049B; Beyotime, China) was used to stain mitochondria for 30 min, for morphology observation. Then, DAPI was used to counterstain the cell nuclei for 5 min. The mitochondrial membrane potential was detected by JC-1 (10 μM). Fluorescence staining of cells was observed with confocal fluorescence microscope (Nikon, Japan). In addition, to quantitatively detect the change of mitochondrial membrane potential, the flow cytometer was used to evaluate JC-1 staining.

2.14. Tube formation assay

First, $1*10^5$ HUVECs were seeded in 6-well plates and cultured with extracts medium for 24 h, and then treated with tBHP for 3 h. After that, $1*10^5$ cells were seeded in Matrigel-coated (#354234; CORNING, USA) 24-well plates for 5 h. Then, the cells were gently rinsed and stained with Calcein for 30 min. At last, the stained cells were observed under fluorescence microscope. Number of junctions and meshs were measured and analyzed by ImageJ 1.8.

2.15. Differentiation of PC12 cells

To evaluate the ability to regulate nerve cell differentiation of hydrogel extracts. Firstly, the SC-conditioned medium should be prepared, SCs that seeded in medium without hydrogel extracts for 1 day and treated with tBHP for 3h. Then, medium with hydrogel extracts were changed for culturing for 3 days and the supernatant was collected and mixed with medium in a ratio of 1:1. Then, PC12 cells were cultured with the SC-conditioned medium in confocal dish and stained with phalloidin (Proteintech, China) and DAPI after being cultured for 5 d. Images were acquired using confocal fluorescence microscope. ImageJ 1.8 software was used to evaluate the percentage of neurite-carrying cells and the length of neurites.

2.16. ALP and ARS staining assays

To evaluate the ability to regulate osteogenic differentiation effect of these hydrogel extracts for BMSCs. Firstly, $1*10^5$ BMSCs were cultured with medium without hydrogel extracts for 1 day and treated with tBHP for 3h. Then, osteogenic medium including hydrogel extracts was changed for culturing with a sustaining time (7 d for ALP staining, and 14 d for ARS staining). For ALP staining, BMSCs were stained with BCIP/NBT ALP color development kit (Beyotime, China). For ARS staining, BMSCs were stained with a 0.1 % ARS solution (Solarbio, China) for 15 min. The images of ALP/ARS staining were obtained with inverted microscope.

2.17. RT-PCR test

Total RNA of different type of cells from these groups was extracted by Trizol reagent (Thermo Fisher, USA) and the concentration was quantified by spectrophotometry. Then, PrimeScript reagent kit was used to performed reverse transcription. At last, RT-PCT was performed to detect the expression level of different genes. The related sequences of primers involved in this study were listed in Table S1.

2.18. Western Blotting

Proteins were extracted from different groups and separated by polyacrylamide electrophoresis according to molecular weight, and then these proteins were transferred to hybridization membranes. These membranes were then blocked by skimmed milk and incubated with relevant diluted primary antibodies against C-JUN (ab40766, Abcam, USA), Calnexin (ab133615, Abcam, USA), anti-VEGF (1:1000; bs-1313R, Bioss), anti-bFGF (1:1000; DF6038, Affinity), anti-Nrf2 (1:1000; #383727, R&D), anti-HO-1 (1:1000; abs131494, Absin), anti-Keap-1 (1:1000; ab118285, Abcam), anti-NGF (1:1000; ab6199, Abcam), anti-S100 (1:1000; ab4066, Abcam), anti-ALP (1:1000; ab154100, Abcam), anti-OCN (1:1000; ab133612, Abcam), anti-RUNX2 (1:1000; ab192256, Abcam) and anti-β-actin (1:5000; ab8226, Abcam). After incubation of primary antibodies was completed, the second antibody was subsequently incubated. The enhanced chemiluminescence detection system was used to observe protein bands and the ImageJ was used to quantitatively analyzed.

2.19. In vivo experiments

STZ (70 mg/kg) was injected to six-week-old SD rats for induction of type I diabetes. Sustaining blood glucose level $\geq$16.7 mM for 10 days was considered to be successful induction of diabetes. Diabetic rats were randomly divided into control, Ag@PEG, Ag@PEG-4OI, Ag@PEG-EXO and Ag@PEG-4OI/EXO hydrogel groups. Then, the infected cranial defect model was prepared based on diabetic rats. Two full-thickness defects with a diameter of 5 mm were made on both side of SD rat skull and gelatin sponges with 100 μL bacteria suspension (108/mL) were placed into the defects for 1 week to induce infection. After that, hydrogels were implanted into the bone defects. Rats from each group were sacrificed at week 1, 4, and 8 post-operated to obtain the skulls. The H&E and Giemsa staining were performed for skulls obtained at week 1 to evaluated the anti-bacteria effect of hydrogels in vivo. The H&E staining, Masson staining and immunohistochemical staining were performed for skulls obtained at week 4 and 8 to evaluated the regeneration of nerve and bone. The primary antibodies were anti-OCN (1:1000; ab93876, Abcam), rabbit anti-CGRP (1:1000; ab81887, Abcam), and rabbit anti-NGF (1:1000; ab216419, Abcam).

2.20. Statistical analysis

Statistical analysis of all data was performed using SPSS version 22.0 (Inc., Chicago, IL, USA). The one-way analysis of variance (ANOVA) and Student's t-tests were used to evaluate the statistical significance between different groups. $P < 0.05$ was accepted as statistical significance, whereas $P > 0.05$ was considered to be not significant (ns).

3. Results

3.1. Preparation and characterization of the hydrogels

To load the EXO of repair SCs, SCs should be firstly transformed into

repair SCs. As shown in figure (Fig. S1), after stimulation with 2 μg/mL TGF-β for 3h, the protein expression of C-JUN increased significantly and the morphology of SCs was obviously changed. Previous studies reported that the genes of Olig1, Shh, artemin, and GDNF would increase after SCs were successfully transformed into repair SCs. Hence, the mRNA expression of Olig1, Shh, artemin, and GDNF was detected. As expected, in the group of repair SCs, the gene expression level of Olig1, Shh, artemin, and GDNF was increased significantly (Fig. S2), which proved that the repair SCs were successfully constructed. Subsequently, to verify if the extraction of EXO was successful, we detected the membrane proteins, particle size and morphology of extracted EXOs. As shown in (Fig. S3), the TSG101 was significantly increased than control group, and the mean particle size was between 30 and 150 nm. The above results proved that the extraction of EXO was successful.

The formation process of hydrogels was shown in Fig. 2A, the 4-arm-PEG-SH solution, whether the 4OI or EXO were contained or not, was liquid statue. Once the $AgNO_3$ solution was added into above solution, gel-like material would be obtained (Fig. 2B). In FTIR analysis, the absorption peak observed near 2874 cm^{-1} in 4-arm-PEG-SH (PEG) powders is possibly attributed to the –SH groups in the PEG powders. Notably, distinct absorption peaks are observed around 2879 cm^{-1} in the Ag@PEG samples, suggesting the formation of coordination bonds between –SH groups in PEG powders and the Ag^+. This shift may be due to the enhanced electron-withdrawing effect of the –SH group caused by coordination interactions. This phenomenon indicates the interaction between Ag^+ and PEG (Fig. S4). A ruler was used to divide hydrogel into two parts, the two parts were fused after 30 s (Fig. 2C). As shown in Fig. 2D, we detected the elastic modulus (G′) and loss modulus (G″) to evaluate the rheological property of hydrogels. The dynamic frequency sweep results showed that G′ was always lower than G″ between the frequency from 0.1 to 10 Hz, which suggested that these hydrogels were self-healing.

The hygroscopicity of hydrogels was shown in Fig. 2E, after immersion these hydrogels into PBS for 12 h, these hydrogels exhibited a similar maximum weight value, showing that the hygroscopicity was not changed with 4OI or EXO added. Hydrogels were almost completely degraded within 12 days (Fig. 2F). As the degradation of hydrogels, the 4OI and Ag^+ were gradually released to regulate the statue of cell in the early process of bone defect repair. As shown in Fig. 2G, the released 4OI in Ag@PEG-4OI group was reached to (52.67 % ± 1.53 %) on day 1 and reached to (88.33 % ± 1.16 %) on day 7, which was similar with Ag@PEG-4OI/EXO group. As shown in Fig. 2H, the release of Ag^+ in every group was similar. The 4OI and EXO would not disturb the degradation function of Ag@PEG hydrogel. In addition, the micro

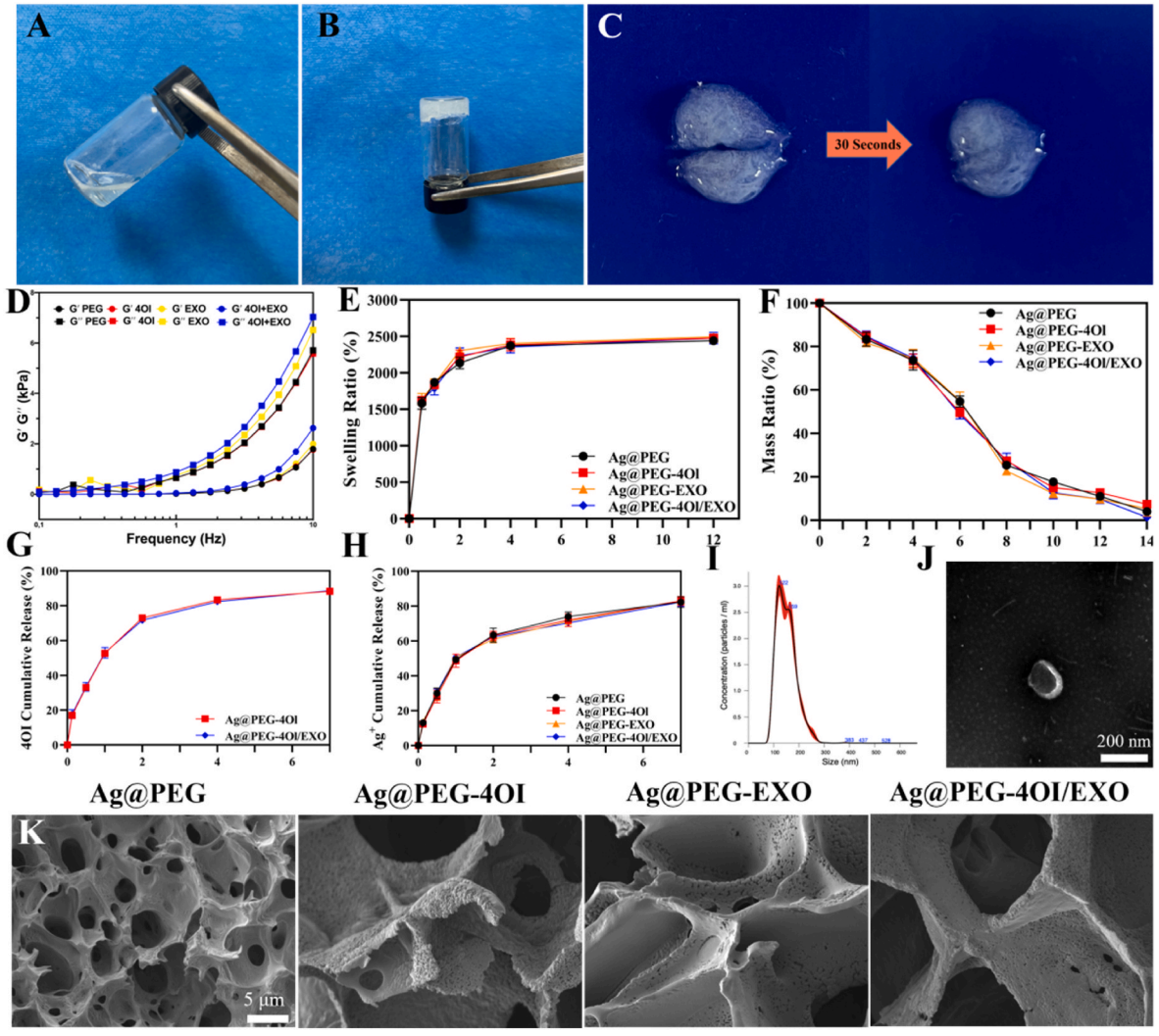

Fig. 2. Characterization and morphology of the hydrogels. (A) Solution of 4-arm-PEH-SH powder dissolved into water. (B) Hydrogel formed after $AgNO_3$ is added. (C) Image depicts the self-healing property of hydrogel. (D) Rheological test, (E) swelling properties, (F) Degradation, (G) 4OI release behavior, (H) Ag^+ release behavior of hydrogels in vitro. (I) and (J) Particle size and SEM morphology identification of extracted EXOs. (K) SEM morphology images of hydrogels. Scale bar = 200 nm in panels (J), 5 μm in panels (K).

morphology of these hydrogels was shown in Fig. 2K. These hydrogels had highly porous internal morphologies, which was benefit for bone regeneration. Once the added of 4OI and EXOs, the pore size was changed.

3.2. In vitro antibacterial evaluation

Escherichia coli (Gram-negative bacterium) and *Staphylococcus aureus* (Gram-positive bacterium) were used to evaluate the antimicrobial effect of hydrogels. The agar plate assay was firstly used to evaluate the antibacterial function of different hydrogel groups. As shown in Fig. 3A, the number of bacterial colonies in control group was more than the other groups. To quantitatively analyze the antibacterial effect, the number of bacterial colony-forming units (CFUs) was counted (Fig. 3B and C). In addition, the live/dead bacterial staining assay was further performed, the living bacteria exhibited green fluorescence while the dead bacteria exhibited red fluorescence. As shown in Fig. 3D and E, there was almost no red fluorescence emitting in control group while the vast majority of bacteria were stained with red in the other groups.

Once the bacteria died, the morphology of bacteria will change [38]. To observe the morphologic change, the SEM was performed to visualize the morphology. As shown in Fig. 3F and G, the bacteria in control group remained normal membrane while the irregular and wrinkled membrane was observed in the other groups.

3.3. In vitro antioxidative and mitochondrial protection properties of hydrogels

The constant oxidative stress is well-known in diabetic microenvironment, which will induce severe inflammation, inhibit angiogenesis and nerve regeneration, resulting in prolonged bone defect repairing [5, 39]. Therefore, the 4OI was loaded in Ag@PEG hydrogel and its antioxidant property was evaluated. As expected, these hydrogels loaded with 4OI had a good scavenging effect on ROS. As shown in Fig. S5, the intracellular green fluorescence in these groups without 4OI was more powerful after treated with tert-butylhydroperoxide (tBHP), in the meantime, the mean fluorescence intensity was higher. We further performed flow cytometry to quantitatively detect ROS level in BMSCs. As shown in Fig. 4A, B, C, the ROS level in groups without 4OI was higher after treated with tBHP, but the ROS level decreased in groups with 4OI.

The flow cytometry was performed to quantitatively detect the JC-1 ratio in different groups, compared with groups with 4OI, the JC-1 ratio was significantly lower (Fig. 4D and E). In addition, the JC-1 fluorescent probe, a sensitive fluorescent sensor, is used to evaluate the effect of the hydrogels on mitochondrial protection by detecting the mitochondrial

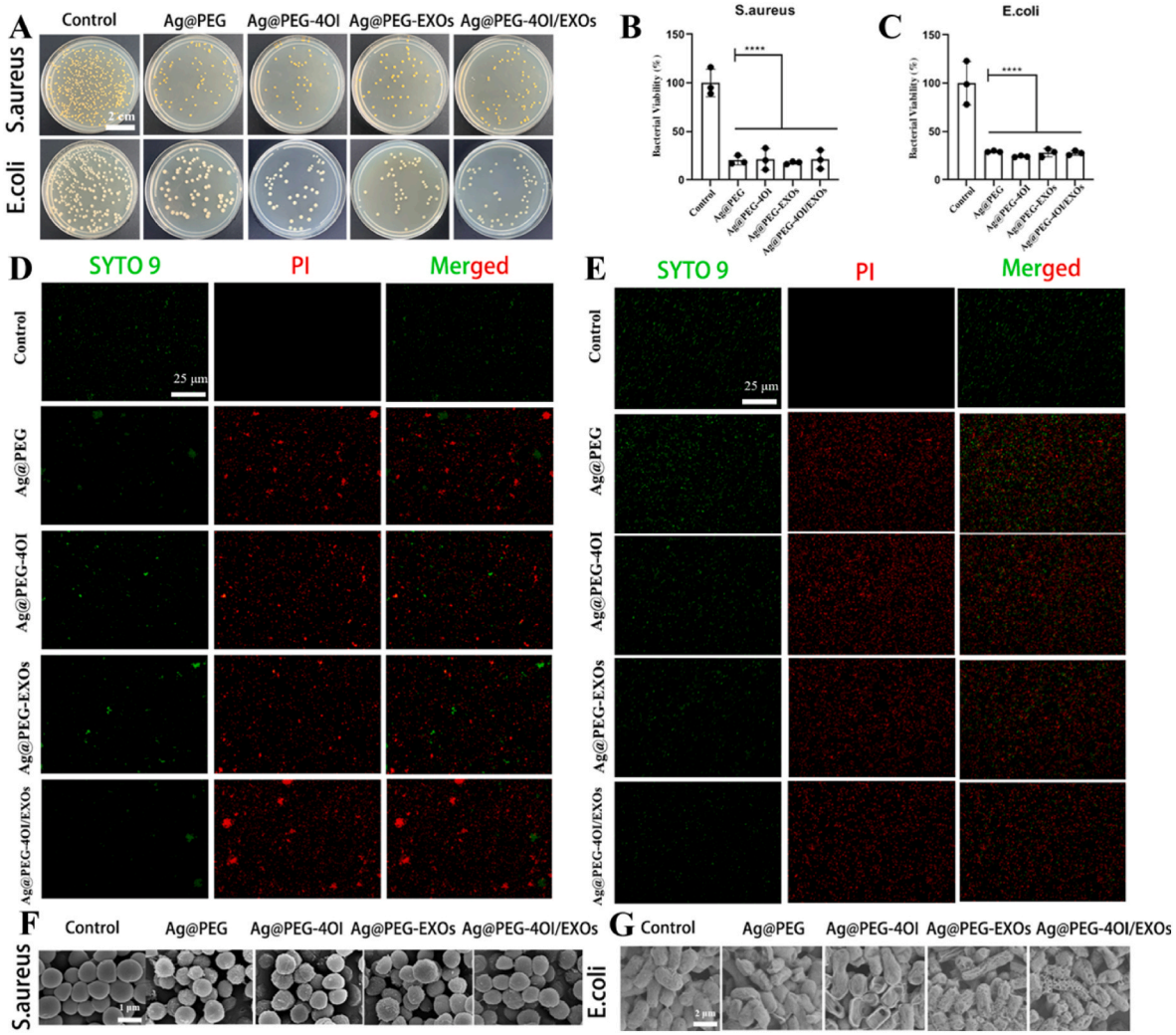

Fig. 3. Evaluation of antibacterial efficiency of hydrogels in vitro. (A) Bacterial colonies grown of S.aureus and E.coli on spread plates in different groups. (B) and (C) Quantification of numbers of S.aureus and E.coli colonies in A. (n = 3). (D) and (E) SYTO 9/PI staining images of S.aureus and E.coli in different hydrogels. (F) and (G) SEM images of S.aureus and E.coli in different hydrogels. Scale bar = 2 cm in panels (A), 25 μm in panels (D, E), 1 μm in panels (F), 2 μm in panels (G). ***P < 0.001.

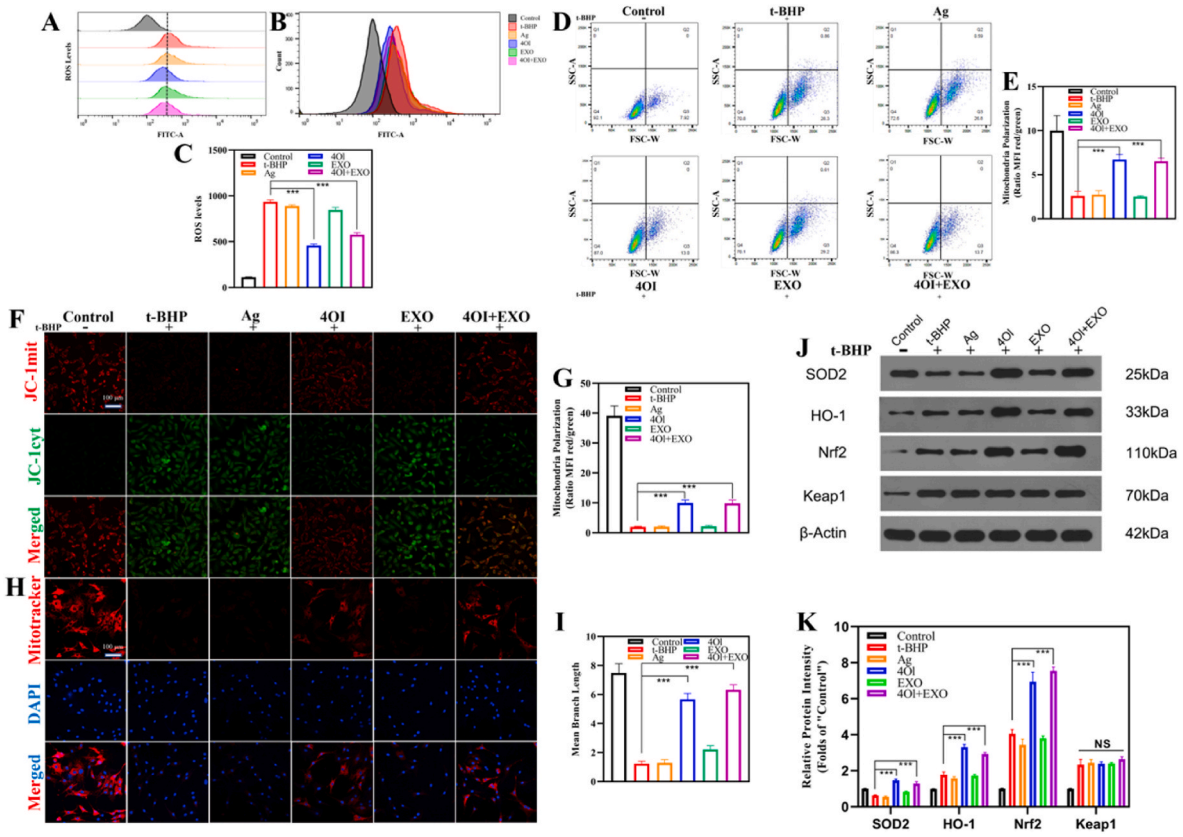

Fig. 4. Evaluation of ROS-scavenging, antioxidant and mitochondrial protection activity of different hydrogels in BMSCs. (A) and (B) Flow cytometry analysis of intracellular ROS levels in BMSCs treated with hydrogels containing different ingredients. (n = 3). (C) Quantitative analysis of A. (n = 3). (D) and (E) Flow cytometry and quantitative analysis of mitochondrial membrane potential levels in BMSCs treated with hydrogels containing different ingredients. (n = 3). (F) Representative fluorescent images illustrating the mitochondrial network by JC-1 staining. (G) Quantitative analysis of mitochondria polatization. (n = 3). (H) Representative images of mitochondrial micrographs by MitoTracker staining. (I) Quantitative analysis of mean branch length of mitochondria. (n = 3). (J) Western blot and (K) quantitative analysis of SOD2, HO-1, Nrf2 and Keap1 in different groups. (n = 3). Every group was treated with tBHP before treated with hydrogels except for control group. Scale bar = 100 μm in panels (F, H). ***P < 0.001.

statue. As shown in Fig. 4F and G, the accumulation and production of green fluorescence intensity were higher in the groups without 4OI, which represented the low mitochondrial membrane potential. Pre-treatment with hydrogels extracts from groups with 4OI effectively restore the mitochondrial function by protecting the mitochondrial membrane potential. Furthermore, the MitoTracker red fluorescent probe was used to detect the mitochondrial morphology. As expected, the MitoTracker images showed that mitochondria almost invisible in the groups without 4OI (Fig, 4H). However, in the groups with 4OI, the morphology of mitochondria was nearly normal. We further quantitatively analyzed the mitochondrial footprint and the mean branch length using the Mitochondrial Network Analysis tool, which was lower in groups without 4OI (Fig, 4I).

In our previous studies, the 4OI could activate Keap1-Nrf2 pathway to restore the angiogenesis ability of HUVECs in diabetic microenvironment. To verify whether this signal pathway is also activated in BMSCs, the level of downstream related gene expression is detected, including Nrf2, HO-1, and Keap1 [40]. Results of Western Blotting test and RT-PCR demonstrated that no significant difference of gene expression of Keap1 between any groups treated with tBHP (Fig. 4J). However, the downstream gene expression such as Nrf2 and HO-1 of Keap1-Nrf2 signal pathway was significant increased (Fig. 4K). Hence, we found that the 4OI also restored the functions of BMSCs via Keap1-Nrf2 pathway.

3.4. In vitro neurogenesis property of the hydrogels

The peripheral nervous system has considerable regenerative ability in that it can repair a fully cut nerve [41]. As shown in Fig. 5A, B, C, all groups performed neurite outgrowth of PC12. Groups with 4OI or EXO had more effective in promoting neurite outgrowth than tBHP and Ag groups, but lower than control group. There was no significant difference between groups of 4OI and EXOs. The Ag@PEG-4OI/EXO group had the best effective in neurite outgrowth. EXO.

SCs could secret neurotrophins, such as nerve growth factor (NGF) and brain-derived neurotrophic factor (BDNF), which regulates the regeneration of nerves. As shown in Fig. 5D, E, F, groups with 4OI or EXO had higher expression of NGF and S100 than tBHP and Ag@PEG groups, but lower than control group. Furthermore, there was no significant difference between groups of Ag@PEG-4OI and Ag@PEG-EXOs. The Ag@PEG-4OI/EXO group had highest gene expression (Fig. 5G and H). Besides, the 4OI might also protect SCs from effect of oxidative stress, yet this part was not studied in this study, which would detect in the further study.

3.5. In vitro angiogenesis property evaluation

Revascularization is also important for nutrient supply at bone defect area [42]. HUVECs were seeded on the conditioned medium of different hydrogels to evaluate the cytocompatibility. Live/dead cellular staining was performed on day 1 and day 3 after seeding, which showed favourable compatibility without toxicity (Fig. 6A). Moreover, the

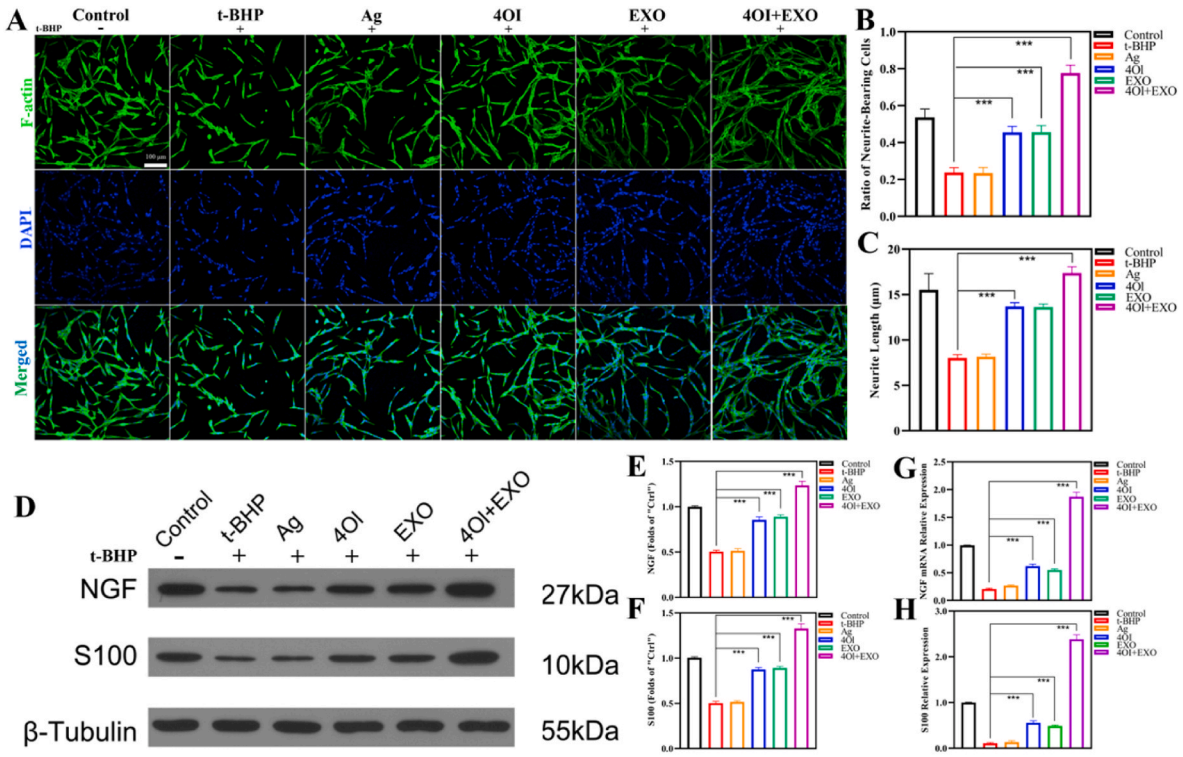

Fig. 5. Nerve regeneration promoting ability of different hydrogels in vitro. (A) F-actin staining images of PC12 cells on day 5 (cells with protrusion length longer than 10 μm are assigned as neurite-bearing cells). (B) Percentage of neurite-bearing cells. (n = 3). (C) quantitative analysis of neurite length. (n = 3). (D) Western blot of NGF and S100. (E) and (F) Quantitative analysis of NGF and S100. (n = 3). (G) and (H) RT-PCR analysis of NGF and S100 mRNA expression. (n = 3). Scale bar = 100 μm in panels (A). ***P < 0.001.

CCK-8 assays were performed to evaluate the cell viability after seeding on hydrogel extracts. As shown in Fig. 6B, there was on significant difference between every groups.

Next, the migration of endothelial cells is the basis of neovascularization. As shown in Fig. 6C and D, the cell migratory rate in these groups without 4OI or EXO was remarkably inhibited, while it was effectively recovered in Ag@PEG-4OI and Ag@PEG-EXO groups. Especially in Ag@PEG-4OI/EXO group, the migratory rate was highest.

To evaluate the effect of the hydrogels in process of angiogenesis, the tube-formation assay was performed. As shown in Fig. 6E, the numbers of tube formation were significantly inhibited in tBHP and Ag@PEG groups, while the inhibition effect of tube formation in group with 4OI or EXO was lower. Especially in Ag@PEG-4OI/EXO group, the formation of mesh number and junction number were highest, even higher than control group (Fig. 6F and G). EXO.

To further quantitively analyze the angiogenesis of these hydrogels in oxidative stress, RT-PCR and western blot assays were performed to detect expression level of angiogenesis genes, such as VEGF and FGF2. As expected, the expression level of VEGF and FGF2 was significantly inhibited in groups without 4OI or EXO (Fig. 6H, I, J). However, in groups with 4OI or EXOs, the expression levels were increased, but lower than control group. The Ag@PEG-4OI/EXO group achieved highest expression effect, even higher than control group (Fig. 6K and L). Ag@PEG-4OI/EXO hydrogel might serve as an ideal agent to facilitate vascularization in oxidative environment.

3.6. In vitro osteogenic property evaluation

BMSCs were seeded in the extract medium of different hydrogels to evaluate the cytocompatibility. Live/dead cellular staining and CCK-8 assays were performed after seeding, which showed favourable compatibility without toxicity (Fig. 7A and B). As shown in Fig. 7B, there was on significant difference between every groups. Hence, these hydrogels were biosafe and cytocompatible.

To evaluate the effect of different hydrogels on osteogenic differentiation of BMSCs, alkaline phosphatase (ALP) staining assay was performed. The results of ALP staining on day 7 showed that Ag@PEG-4OI/EXO group had the best differentiation property, even higher than control (Fig. 7C). The groups with 4OI or EXO had higher effect than Ag and tBHP groups, but there was no significant difference between them. To evaluate the effect of extracellular matrix mineralization in different groups, the Alizarin red S (ARS) staining, indication of late osteogenic differentiation, was performed in day 14 after seeding. As shown in Fig. 7D, the Ag@PEG-4OI/EXO group achieved the best effective in calcium deposition areas. The tBHP and Ag groups achieved the lowest effect. The groups with 4OI or EXO were increased, but lower than control group.

To quantitively evaluate the effect of osteogenic differentiation, the western blot (Fig. 7E, F, G) was performed detect the ALP and osteocalcin (OCN), and RT-PCR (Fig. 7H, I, J, K) was performed to detect the gene expression of ALP, collagen type I (CoL-I), runt-related transcription factor 2 (Runx-2) and OCN. As shown in Fig. 7H, I, J, K, the Ag@PEG-4OI/EXO group achieved the highest expression level compared to that in the other groups.

3.7. In vivo antibacterial evaluation

To evaluated the anti-bacteria effect of hydrogels in vivo, the agar plate assay, Hematoxylin and Eosin (H&E) and Giemsa staining were performed after one week of hydrogels placed into infected bone defect (Fig. 8A). As shown in Fig. 8B and C, the number of bacterial colonies in control group that not placed with hydrogel was more than the other groups. And in the control group, H&E and Giemsa staining were observed with worse inflammation and more bacteria than other groups (Fig. 8A).

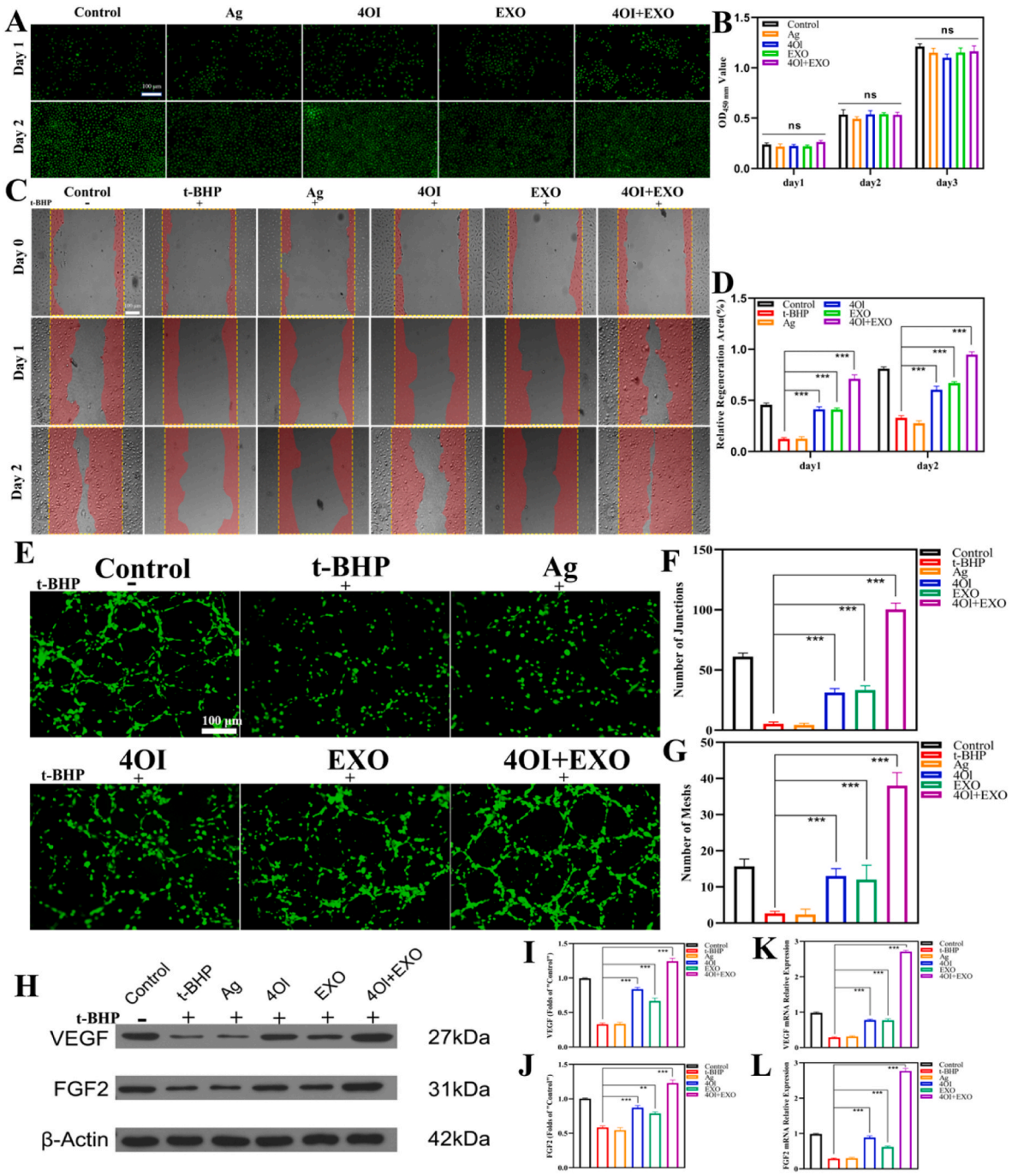

Fig. 6. Evaluation of cytotoxicity and angiogenic ability of different hydrogels in HUVECs. (A) Live/dead staining images of HUVECs in hydrogels containing different ingredients for 1 and 2 days. (B) CCK-8 quantitative results for culturing with hydrogels in day 1, day 2 and day 3. (n = 3). (C) Images of wound-healing in different hydrogel treatment groups at day 1 and day 2. (D) Quantitative analysis of C. (n = 3). (E) Representative tube-formation images of HUVECs in vitro in different groups. (F) and (G) Quanyitative analysis of number of junctions and number of meshs of the formed tube in E. (n = 3). (H) Western blot of VEGF and FGF2. (I) and (J) Quantitative analysis of VEGF and FGF2. (n = 3). (K) and (L) RT-PCR analysis of VEGF and FGF2. (n = 3). Scale bar = 100 μm in panels (A, C, E). **P < 0.01, ***P < 0.001.

3.8. *In vivo neurogenesis and osteogenic properties of hydrogels*

The detections of micro-computed tomography (micro-CT) and histology were performed to analyzed the effect of different hydrogels on bone defect repair at 4 and 8 weeks after implantation. As shown in Fig. 8D and E, the control group showed the worst effect of bone regeneration because the uncleared bacteria and oxidative stress whether in week 4 or week 8. In contrast, as long as groups with the hydrogel implantation, the bone regeneration condition was improved owing to the antibacterial effect of Ag^{+}. The Ag@PEG-4OI/EXO group achieved the best effect in bone regeneration. The bone-to-tissue volume ratio (BV/TV) in the Ag@PEG-4OI/EXO group was significantly greater than that in the others whether in week 4 or week 8 (Fig. 8D and E). Histological results at week 4 and 8 showed that the groups with 4OI or EXO had bone regeneration, but the Ag@PEG-4OI/EXO group achieved the best new bone formation (Fig. 8F and G). In addition, to evaluate the expression of OCN in vivo, an osteogenic marker, the immunofluorescence staining was performed. The Ag@PEG-4OI/EXO group showed

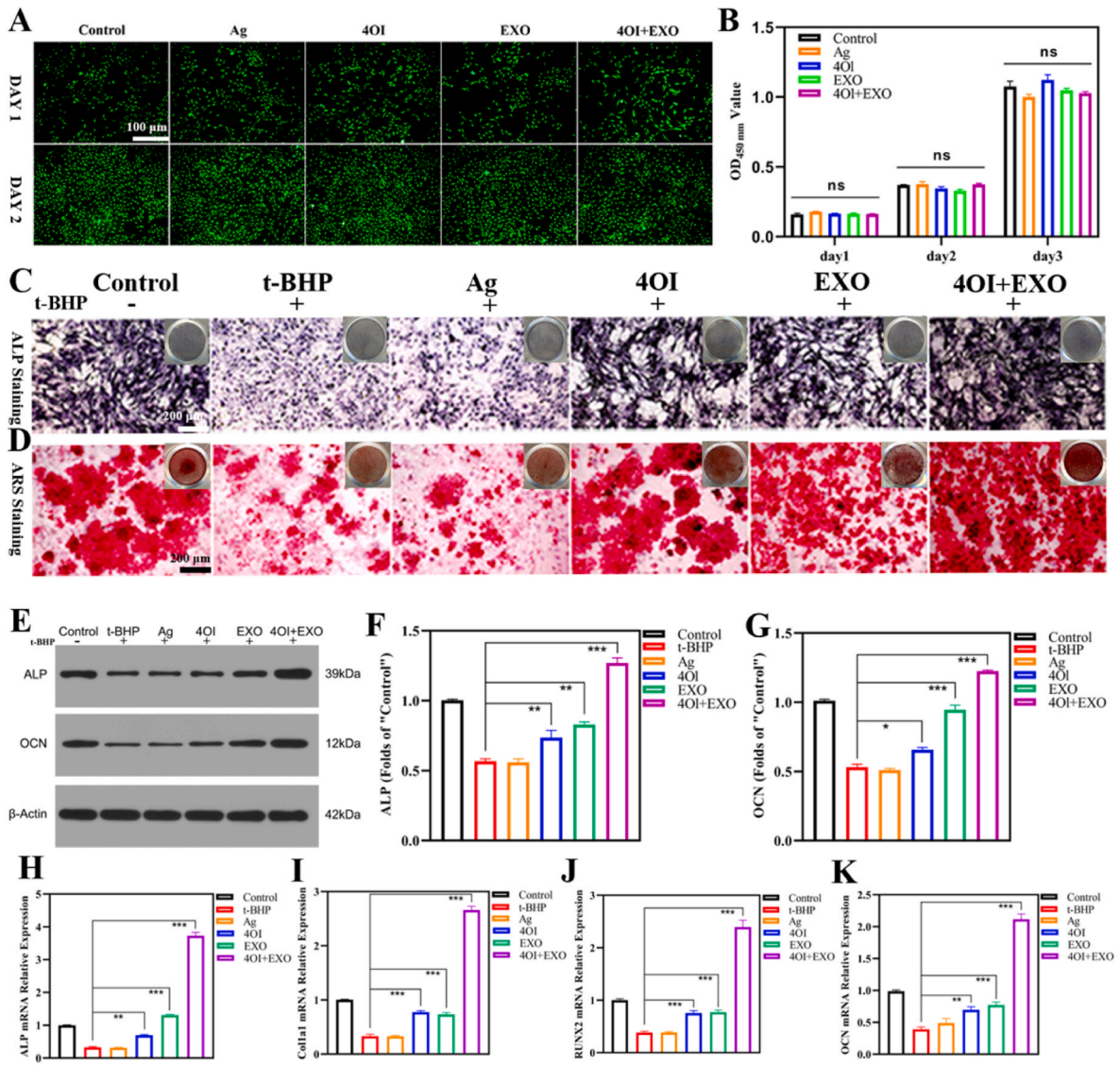

Fig. 7. Osteogenic bioactivities of different hydrogels in vitro. (A) Live/dead staining images of BMSCs in hydrogels containing different ingredients for 1 and 2 days. (100 μm) (B) CCK-8 quantitative results for culturing with hydrogels in day 1, day 2 and day 3. (n = 3). (C) ALP staining assay on day 7 after culturing with different hydrogels. (D) ARS staining of matric mineralization on day 14. (E) Western blot of ALP and OCN. (F) and (G) Quantitative of ALP and OCN. (n = 3). (H)–(K) RT-PCR analysis of ALP, OCN, Col1a1 and RUNX2 mRNA expression. (n = 3). Scale bar = 100 μm in panels (A), 200 μm in panels (C, D). *P < 0.05, **P < 0.01, ***P < 0.001.

the highest expression level compared to the other groups (Fig. 9A–D). EXO.

In the process of bone regeneration, nerves play a crucial role in initiating and regulating, whether these hydrogels can promote the growth of nerve in vivo needs to be further explored. Hence, the immunofluorescence staining for NGF was performed. As shown in Fig. 9B–E, the expression of NGF in control groups was lowest. The highest expression of NGF was observed in group both with 4OI and EXOs. As same with the expression of NGF, the Ag@PEG-4OI/EXO group had the highest expression level of CGRP (Fig. 9C–F). These above results confirmed that the Ag@PEG-4OI/EXO hydrogel possessed the effect in promoting neural network reconstruction.

4. Discussion

Bone grafted biomaterials transplanted at the bone defect play a vital role to change the functions of cells to improve the bone regeneration [7, 43]. Recently, the engineering hydrogel biomaterials are popularly applied owing to its efficient to assist bone regeneration [44,45], which becomes a promising method. For these hydrogels, it is indispensable to change the severe microenvironment to ensure the normal function of local cells, to improve the ability of tissue regeneration. Therefore, in this study, based on the hydrogel formed by the cross linked between Ag^+ and 4-arm-PEG-SH to load 4OI and EXOs. The property of self-healing allows local restriction of hydrogels and incorporated biological compounds, resulting in higher and more sustained effective doses. In the antibacterial tests, it was found that the Ag^+ contained in the hydrogel had relatively effective antibacterial ability. In the oxidative stress BMSCs model induced by t-BHP, the medium containing 4OI hydrogel extract can effectively protect the mitochondrial membrane potential and prevent the cells from oxidative stress injury by Keap1-Nrf2 pathway. At the same time, hydrogels containing 4OI or EXO had ideal effects on promoting nerve growth, angiogenesis and osteogenic differentiation. In the diabetic infected bone defect model, it was also found that hydrogels with 4OI or EXO could effectively improve tissue regeneration. Hence, the Ag@PEG-4OI/EXO hydrogel with excellent antibacterial and antioxidative properties was prepared.

The stable physical and chemical microenvironment in the bone defect is the basis for the bone reconstruction. However, in the diabetic and infected bone regeneration microenvironment, the excess ROS will

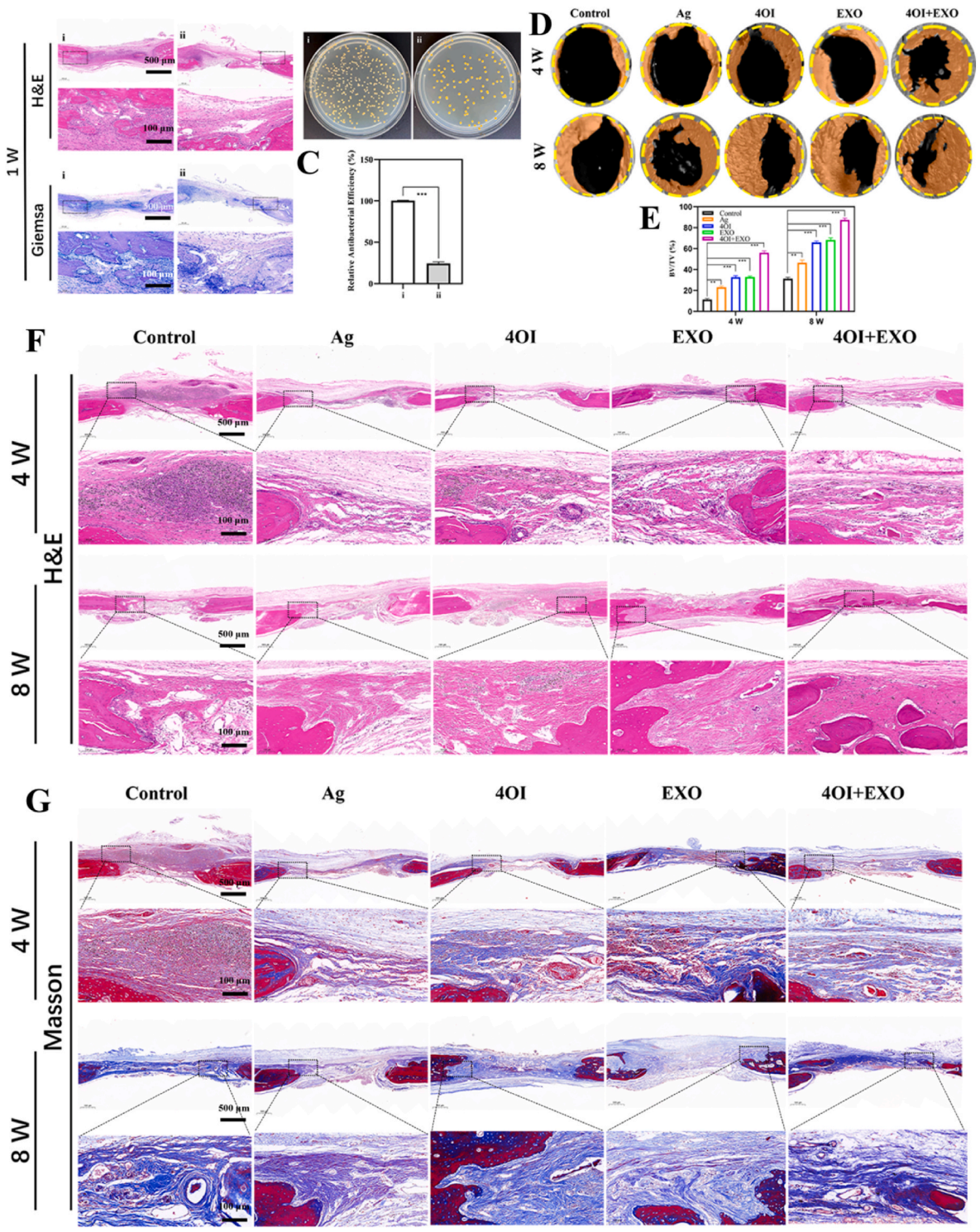

Fig. 8. In vivo antibacterial and osteogenic properties of different hydrogels. (A) H&E and Giemsa staining images after hydrogels placement at week 1. (B) Spread plate assays and (C) quantitative analysis of antibacterial efficiency against S.aureus after hydrogels placement at week 1 in vivo. (n = 3). (D) Micro-CT images and (E) quantitative analysis of diabetic infected bone defects treated with hydrogels at week 4 and week 8. (n = 3). (F) H&E and (G) Masson staining at week 4 and week 8. Scale bar = 500 μm in standard panels, 100 μm in magnified panels. **P < 0.01, ***P < 0.001.

inhibit the reconstruction of surrounding tissue, including nerves, vessels and bone [46]. In this study, the Ag^{+} was used as cross-linking agent to form hydrogel. The Ag^{+} could affect the potential of bacteria to interfered with the synthesis of bacterial wall, impede the synthesis of protein and nucleic acid, which would play a role in antibacterial [47]. *Escherichia coli* (Gram-negative bacterium) and *Staphylococcus aureus* (Gram-positive bacterium) were two of the most commonly involved bacteria in bone infection [48], therefore, the above bacteria were used to evaluate the antimicrobial effect of hydrogels in this study. In this study, Ag@PEG hydrogel itself has antibacterial effect owing to Ag^{+}, and the antibacterial effect of AG@PEG will not be affected after loading 4OI or EXOs, because the in vivo and in vitro antibacterial test effects of all hydrogel groups are basically similar. However, after the successful removal of bacteria, the high ROS diabetes microenvironment also

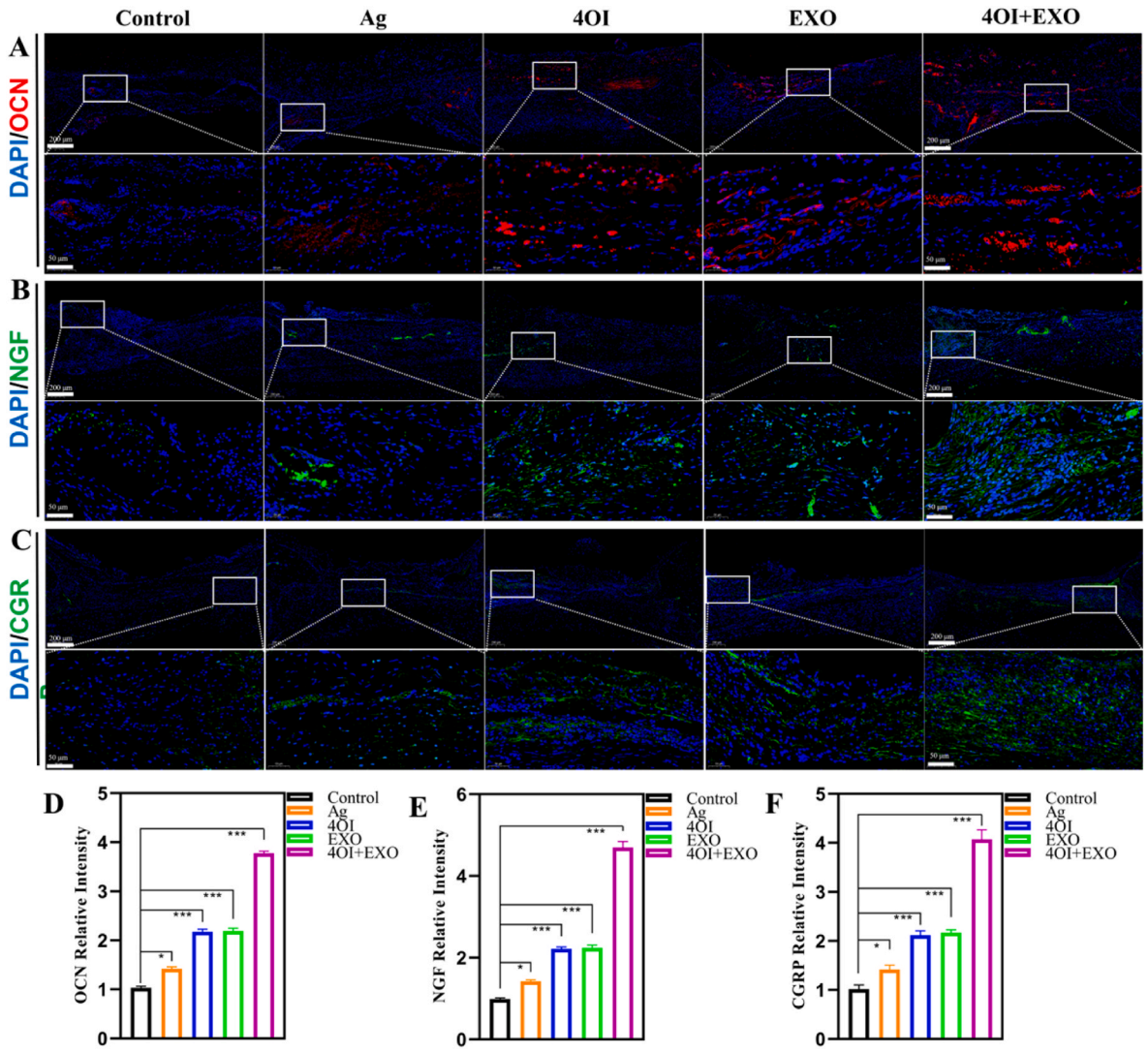

Fig. 9. Immunofluorescence staining analysis of innervation and ossification in vivo. (A) Immunofluorescence staining images of OCN at week 4 expression. (B) Immunofluorescence staining images of NGF at week 4 expression. (C) Immunofluorescence staining images of CGRP at week 4. (D)–(F) Quantitative analysis of OCN, NGF and CGRP expression level. (n = 3). Scale bar = 200 μm in standard panels, 50 μm in magnified panels. *P < 0.05, ***P < 0.001.

needs attention.

The constant oxidative stress is well-known in diabetic microenvironment, inducing severe inflammation, which inhibits angiogenesis, nerve and bone regeneration, resulting in prolonged repair of bone defect [5]. Endowing the Ag@PEG hydrogel with effective antioxidant property is a meaningful way to improve the function of bone regeneration. Therefore, the 4OI is loaded in Ag@PEG hydrogel and the antioxidant property is evaluated. Normal mitochondrial function plays an important role in keeping cell functions, especially in microenvironment with excess ROS [49]. Diabetic microenvironment induced mitochondrial dysfunction is the primary cause of ROS increasing, the produced ROS will damage mitochondrial membrane potential and lead to abnormality of functions [50]. In this study, our results found that the hydrogels containing 4OI could reverse the mitochondrial membrane potential, the Ag@PEG-4OI and Ag@PEG-4OI/EXO groups had higher mitochondria polarization than t-BHP and Ag@PEG groups. Besides, the mean branch length of mitochondria was longer in Ag@PEG-4OI and Ag@PEG-4OI/EXO groups. But the underlying mechanism was unclear.

As reported by previous studies that 4OI could alkylate Keap1, leading the activity of Keap1-Nrf2 pathway and boosting downstream related gene expression [28]. The increased expression of Nrf2 in cells leads to the increasing of NADPH dehydrogenase quinone 1 (NOQ1) and glutathione reductase and protects the mitochondrial membrane potential, ultimately resulting in enhancing the antioxidant capacity of cells [34]. Recently, Ding et al. reported that the 4OI could protect mitochondria from oxidative stress injury and restore the endothelial cell functions to nearly normal level in the excess ROS microenvironment [18]. In this study, we found that the 4OI also restored the functions of BMSCs via Keap1-Nrf2 pathway because the expression of Nrf2, HO-1, SOD2 was increased.

The peripheral nervous system (PNS) has considerable regenerative ability in that it can repair a fully cut nerve [35]. Peripheral nerves consist of bundles of axons, with each axon associated and enveloped by repair SCs, the main glial cell of the PNS. Once the peripheral nerve was injured, the repair SCs would migrate collectively to guide regrowing axons across a 'bridge' of new tissue, and form tube-like structures within their original basement membranes, acting as "tunnels'' to direct the regrowing axons back to their original target [23]. Hence, in this study, we successfully constructed the repair SCs and extracted its EXOs. Whether in vitro or in vivo experiments, the hydrogel with EXO improved the regeneration of nerve and promote the NGF expression. These results were similar to the previously published reports [36]. Besides, in vivo experiment, the regenerated nerves could further improve the healing of bone defect because the nerve was proved as the

initiator of bone regeneration. However, the growth situation was similar between Ag@PEG-4OI and Ag@PEG-EXO groups, which might be that the 4OI also protected the PC12 from oxidative stress injury and the promoting role of EXOs. The specific mechanism would be studied in our subsequent study.

Revascularization is also important for nutrient supply at bone defect area. However, as mentioned by previous studies [37], the normal functions of endothelial cells, such as angiogenesis and migration, were inhibited by oxidative stress in diabetic microenvironment [51]. With the application of the antioxidant hydrogels, the functions of angiogenesis and migration were restored, which was important in bone defect repair. In this study, we found that the 4OI and EXO both improve the tube forming in excess ROS microenvironment, the results were similar to previous published reports. Because the 4OI protected the weak cells from oxidative stress injury, and the EXO could improve the gene expression of angiogenesis.

Osteogenesis is a complex and dynamic process, the microenvironment where the BMSCs cultured plays a key role in the process of cell proliferation, differentiation and mineralization [52]. We noted that the Ag@PEG-4OI and Ag@PEG-EXO groups both had better bone defect repairing effect, but the repairing effect was worse than control group. Benefiting from 4OI and EXOs, in the excess ROS microenvironment, the 4OI protected the BMSCs from oxidative stress injury to restored the cell function to nearly normal and the EXO could improve the cell functions. Perhaps the 4OI or EXO alone could not recover the osteogenic differentiation ability of BMSCs and repairing effect to normal level. Hence, in this study, the Ag@PEG-4OI/EXO group achieved the best bone regeneration, the Ag@PEG-4OI and Ag@PEG-EXO groups achieved the better bone regeneration than t-BHP and Ag@PEG groups yet worse than control group whether in vivo or vitro.

In the developing skeleton, sensory neurons innervate the perichondrium of the developing bones at sites of NGF production where they are required for subsequent bone progenitor cell differentiation and mineralization [7]. In the process of bone regeneration, nerves play a crucial role in initiating and regulating, which mediate the interaction with bone according to secreting CGRP. Some studies have confirmed that the $CGRP^{+}$ sensory nerves sprouted in the process of bone regeneration [13]. In this study, we detected the expression of NGF and CGRP in animal model. We found that the Ag@PEG-4OI/EXO group achieved the best bone healing and the expression of NGF and CGRP were also highest, perhaps the regenerated nerve promoted the bone regeneration. These results proved that the inseparable relation between nerve and bone.

Our study provided a multifunctional hydrogel for the treatment of diabetic infected bone defect and verified the properties in antibacterial, anti-oxidant, mitochondrial protection and regeneration of nerves and bone. However, some limitations were existing in this study. The constructed hydrogel could not perform controlled release of loaded active substances. Besides, this study focused on the treatment of diabetic infected bone defect, the concrete crosstalk mechanism between nerves and bone was not studied. In the future, the related studies would be further performed to solve the limitations in above.

5. Conclusion

We successfully developed a multifunctional, biocompatible and biodegradable Ag@PEG-4OI/EXO hydrogel for diabetic infected bone defect. The hydrogel performed efficient antibacterial property under the role of Ag^{+}, and the 4OI performed efficient roles of ROS eliminating and mitochondrial protection by Keap1-Nrf2 pathway, which synergistically created favourable microenvironment for diabetic infected bone defect with EXOs. Besides, the Ag@PEG-4OI/EXO hydrogel could efficiently promote the regeneration of nerves and bone tissue whatever it is in vitro or in vivo. In summary, this study provided a novel strategy for the treatment of diabetic infected bone defect by loading 4OI and EXOs, eliminating excess ROS and protecting mitochondrial functions to promoting regeneration of nerve and bone.

CRediT authorship contribution statement

Yizhou Wan: Writing – review & editing, Writing – original draft. **Qing Gao:** Data curation, Conceptualization. **Bing Ye:** Investigation, Formal analysis. **Wenzhe Sun:** Methodology. **Kaifang Chen:** Supervision. **Xiaodong Guo:** Visualization, Resources, Funding acquisition.

Ethics approval and consent to participate

The animal experiments were approved by the Use Committees of the Huazhong University of Science and Technology with Protocol numbers: IACUC-3891.

Consent for publication

Data/manuscript publication was approved by all authors. This manuscript does not contain data from any individual person.

Funding

This work was financially supported by the National Natural Science Foundation of China (82272460).

Declaration of competing interest

The authors declare the following financial interests/personal relationships which may be considered as potential competing interests: Xiaodong Guo reports administrative support was provided by National Natural Science Foundation of China. If there are other authors, they declare that they have no known competing financial interests or personal relationships that could have appeared to influence the work reported in this paper.

Acknowledgements

No.

Appendix A. Supplementary data

Supplementary data to this article can be found online at https://doi.org/10.1016/j.mtbio.2025.101588.

Data availability

Data will be made available on request.

References

[1] M. Boni-Schnetzler, D.T. Meier, Islet inflammation in type 2 diabetes, Semin. Immunopathol. 41 (4) (2019) 501–513.
[2] P. Saeedi, I. Petersohn, P. Salpea, et al., Global and regional diabetes prevalence estimates for 2019 and projections for 2030 and 2045: results from the international diabetes federation diabetes atlas, Diabetes Res Clin Pr (2019) 157, 9th edition.
[3] Z.R. Wu, J.X. Bai, G.R. Ge, et al., Regulating macrophage polarization in high glucose microenvironment using lithium-modified bioglass-hydrogel for diabetic bone regeneration, Adv Healthc Mater 11 (13) (2022).
[4] X. Sun, Z.J. Ma, X. Zhao, et al., Three-dimensional bioprinting of multicell-laden scaffolds containing bone morphogenic protein-4 for promoting M2 macrophage polarization and accelerating bone defect repair in diabetes mellitus, Bioact. Mater. 6 (3) (2021) 757–769.
[5] D. Wang, Y.J. Wang, D.Y. Song, et al., Microgels-Encapsulated Magnesium/Emodin-based metal organic framework nanorods for diabetic bone regeneration, Chem Eng J (2024) 487.
[6] Q. Gao, Y. Jiang, D. Zhou, et al., Advanced glycation end products mediate biomineralization disorder in diabetic bone disease, Cell Rep Med 5 (9) (2024) 101694.

[7] A. Marrella, T.Y. Lee, D.H. Lee, et al., Engineering vascularized and innervated bone biomaterials for improved skeletal tissue regeneration, Mater. Today 21 (4) (2018) 362–376.
[8] Z. Li, C.A. Meyers, L.L. Chang, et al., Fracture repair requires TrkA signaling by skeletal sensory nerves, J. Clin. Investig. 129 (12) (2019) 5137–5150.
[9] Y.L. Su, Q. Gao, R.L. Deng, et al., Aptamer engineering exosomes loaded on biomimetic periosteum to promote angiogenesis and bone regeneration by targeting injured nerves via JNK3 MAPK pathway, Mater Today Bio (2022) 16.
[10] R.E. Tomlinson, Z. Li, Q. Zhang, et al., NGF-TrkA signaling by sensory nerves coordinates the vascularization and ossification of developing endochondral bone, Cell Rep. 16 (10) (2016) 2723–2735.
[11] S.T. Guo, C.L. He, Bioprinted scaffold remodels the neuromodulatory microenvironment for enhancing bone regeneration, Adv. Funct. Mater. 33 (40) (2023).
[12] X.B. Zhao, G.F. Wu, J. Zhang, et al., Activation of CGRP receptor-mediated signaling promotes tendon-bone healing, Sci. Adv. 10 (10) (2024).
[13] Q.S. Jiang, L.M. Zhou, Y. Yang, et al., Injectable NGF-loaded double crosslinked collagen/hyaluronic acid hydrogels for irregular bone defect repair via neuro-guided osteogenic process, Chem Eng J 497 (2024).
[14] D.P. Lew, F.A. Waldvogel, Osteomyelitis, Lancet 364 (9431) (2004) 369–379.
[15] M. Vallet-Regí, D. Lozano, B. González, et al., Biomaterials against bone infection, Adv Healthc Mater 9 (13) (2020).
[16] B.E. Nie, S.C. Huo, X.H. Qu, et al., Bone infection site targeting nanoparticle-antibiotics delivery vehicle to enhance treatment efficacy of orthopedic implant related infection, Bioact. Mater. 16 (2022) 134–148.
[17] Q. Zhang, W. Chen, G. Li, et al., A factor-free hydrogel with ROS scavenging and responsive degradation for enhanced diabetic bone healing, Small 20 (24) (2024) e2306389.
[18] E.M. Schuster, M.W. Epple, K.M. Glaser, et al., TFEB induces mitochondrial itaconate synthesis to suppress bacterial growth in macrophages, Nat. Metab. 4 (7) (2022), 856-+.
[19] X.Y. Wu, X. Yi, B.X. Zhao, et al., The volume regulated anion channel VRAC regulates NLRP3 inflammasome by modulating itaconate efflux and mitochondria function, Pharmacol. Res. 198 (2023).
[20] S.T. Liao, C. Han, D.Q. Xu, et al., 4-Octyl itaconate inhibits aerobic glycolysis by targeting GAPDH to exert anti-inflammatory effects, Nat. Commun. 10 (2019).
[21] Q.Y. Ding, T.F. Sun, W.J. Su, et al., Bioinspired multifunctional black phosphorus hydrogel with antibacterial and antioxidant properties: a stepwise countermeasure for diabetic skin wound healing, Adv Healthc Mater 11 (12) (2022).
[22] E.L. Mills, D.G. Ryan, H.A. Prag, et al., Itaconate is an anti-inflammatory metabolite that activates Nrf2 via alkylation of KEAP1, Nature 556 (7699) (2018), 113-+.
[23] H. Liu, Y. Feng, M. Xu, et al., Four-octyl itaconate activates Keap1-Nrf2 signaling to protect neuronal cells from hydrogen peroxide, Cell Commun. Signal. 16 (2018).
[24] L.D. Huyer, S. Mandla, Y.F. Wang, et al., Macrophage immunomodulation through new polymers that recapitulate functional effects of itaconate as a power house of innate immunity, Adv. Funct. Mater. 31 (6) (2021).
[25] E.Y. Kim, H.Y. Shin, J.Y. Kim, et al., ATF3 plays a key role in kdo -lipid A-induced TLR4-dependent gene expression via NF-κB activation, PLoS One 5 (12) (2010).
[26] Y.R. Wang, X.X. Zhang, X.X. Chen, et al., Enhancement of bone repair in diabetic rats with metformin-modified silicified collagen scaffolds, Adv Healthc Mater 14 (3) (2025) e2401430.
[27] X. Zhao, W. Zhang, J. Fan, et al., Application of mesenchymal stem cell exosomes in the treatment of skin wounds, Smart Materials in Medicine 4 (2023) 578–589.
[28] G.R. Ge, W. Wang, Q. Wang, et al., Extracellular vesicle clicking on osteoimplants through biomimetic molecular adhesion enables immune-enhanced osseointegration in diabetics, Adv. Funct. Mater. 34 (27) (2024).
[29] A.L. Cattin, J.J. Burden, L. Van Emmenis, et al., Macrophage-induced blood vessels guide Schwann cell-mediated regeneration of peripheral nerves, Cell 162 (5) (2015) 1127–1139.
[30] J.F. Pan, M. Zhao, X.J. Yi, et al., Acellular nerve grafts supplemented with induced pluripotent stem cell-derived exosomes promote peripheral nerve reconstruction and motor function recovery, Bioact. Mater. 15 (2022) 272–287.
[31] J. Shen, Y. Sun, X. Liu, et al., Nerve regeneration potential of antioxidant-modified black phosphorus quantum dots in peripheral nerve injury, ACS Nano 18 (34) (2024) 23518–23536.
[32] P.J. Arthur-Farraj, C.C. Morgan, M. Adamowicz, et al., Changes in the coding and non-coding transcriptome and DNA methylome that define the Schwann cell repair phenotype after nerve injury, Cell Rep. 20 (11) (2017) 2719–2734.
[33] K.R. Jessen, P. Arthur-Farraj, Repair Schwann cell update: adaptive reprogramming, EMT, and stemness in regenerating nerves, Glia 67 (3) (2019) 421–437.
[34] S. Kim, J.C. Maynard, A. Strickland, et al., Schwann cell O-GlcNAcylation promotes peripheral nerve remyelination via attenuation of the AP-1 transcription factor JUN, P Natl Acad Sci USA 115 (31) (2018) 8019–8024.
[35] Q.Y. Ding, X.R. Jing, S. Yao, et al., Multifunctional hydrogel loaded with 4-octyl itaconate exerts antibacterial, antioxidant and angiogenic properties for diabetic wound repair, Biomater. Adv. 139 (2022).
[36] K.R. Jessen, R. Mirsky, The repair Schwann cell and its function in regenerating nerves, J Physiol-London 594 (13) (2016) 3521–3531.
[37] X.Y. Mao, R.Y. Cheng, H.B. Zhang, et al., Self-healing and injectable hydrogel for matching skin flap regeneration, Adv. Sci. 6 (3) (2019).
[38] D.M. Black, A.R. Thompson, R. Eastell, et al., Bone mineral density as a surrogate endpoint for fracture risk reduction in clinical trials of osteoporosis therapies: an update on SABRE, Lancet Diabetes Endo 12 (6) (2024) 371–373.
[39] W.H. Li, H.W. Zhu, J.Z. Chen, et al., PsAF5 functions as an essential adapter for PsPHB2-mediated mitophagy under ROS stress in, Nat. Commun. 15 (1) (2024).
[40] D. Olagnier, A.M. Brandtoft, C. Gunderstofte, et al., Nrf2 negatively regulates STING indicating a link between antiviral sensing and metabolic reprogramming, Nat. Commun. 9 (2018).
[41] Y.R. Yu, B.H. Jin, J.H. Chen, et al., Nerve-on-a-Chip derived biomimicking microfibers for peripheral nerve regeneration, Adv. Sci. 10 (20) (2023).
[42] J. Hu, S. Dziumbla, J.H. Lin, et al., Inhibition of soluble epoxide hydrolase prevents diabetic retinopathy, Nature 552 (7684) (2017), 248-+.
[43] H. Cui, W. Zhu, B. Holmes, et al., Biologically inspired smart release system based on 3D bioprinted perfused scaffold for vascularized tissue regeneration, Adv. Sci. 3 (8) (2016) 1600058.
[44] R. Boni, A. Ali, A. Shavandi, et al., Current and novel polymeric biomaterials for neural tissue engineering, J. Biomed. Sci. 25 (1) (2018) 90.
[45] X. Jing, C. Xu, W. Su, et al., Photosensitive and conductive hydrogel induced innerved bone regeneration for infected bone defect repair, Adv Healthc Mater 12 (3) (2023) e2201349.
[46] J. Jin, X. Xia, C. Ruan, et al., GAPDH-silence microsphere via reprogramming macrophage metabolism and eradicating bacteria for diabetic infection bone regeneration, J Nanobiotechnology 22 (1) (2024) 517.
[47] Y. Lin, L. Liu, J. He, et al., Rapid release of high-valent silver ions from water-soluble porphyrin complexes to enhance the direct killing of Methicillin-Resistant Staphylococcus aureus, Acta Biomater. 192 (2025) 419–430.
[48] S. Ghosh, M. Sinha, R. Samanta, et al., A potent antibiotic-loaded bone-cement implant against staphylococcal bone infections, Nat. Biomed. Eng. 6 (10) (2022) 1180–1195.
[49] S.J. Chen, W.Z. Lei, Q. Liu, et al., Silk-based nanocomposite hydrogel balances immune homeostasis via targeting mitochondria for diabetic wound healing, Chem Eng J 498 (2024).
[50] M. Wang, D. Yang, L. Li, et al., A dual role of mesenchymal stem cell derived small extracellular vesicles on TRPC6 protein and mitochondria to promote diabetic wound healing, ACS Nano 18 (6) (2024) 4871–4885.
[51] J. Ren, C. Wang, H. Gao, et al., Multitasking asynchronous collaborative nanosystem for diabetic wound healing based on hypoglycemic, antimicrobial, and angiogenesis-promoting effects, Adv Healthc Mater (2024) e2403282.
[52] K. Liu, L. Li, J. Chen, et al., Bone ECM-like 3D printing scaffold with liquid crystalline and viscoelastic microenvironment for bone regeneration, ACS Nano 16 (12) (2022) 21020–21035.